

Highlights

Micro-CT Imaging of *Ex-Vivo* Rat Stomachs: A Detailed Protocol with Comparative Analysis

Savindi Wijenayaka,Alys R. Clark,Dane Gerneke,Recep Avci,Leo K. Cheng,Peng Du

- Phosphotungstic acid (PTA) performs significantly better than Iodine based stains for visualizing soft tissue of rodent stomach.
- Fixative duration does not have a significant impact on tissue contrast within the observed time period of 3-17 weeks, hence using a staining time of 3 weeks is sufficient.
- Optimal staining duration observed lies between seven and nine weeks. Longer staining durations causes the tissue to tear.
- The staining protocol achieved uniform coverage across the stomach, despite minor regional variations in tissue thickness.
- Substantial tissue shrinkage is observed with a quantified volume reduction of $51.56 \pm 5.75\%$.

Micro-CT Imaging of *Ex-Vivo* Rat Stomachs: A Detailed Protocol with Comparative Analysis*

Savindi Wijenayaka^{a,**}, Alys R. Clark^a, Dane Gerneke^a, Recep Avci^a, Leo K. Cheng^{a,b} and Peng Du^{a,*}

^aAuckland Bioengineering Institute, University of Auckland, Auckland 1010, New Zealand

^bDepartment of Surgery, Vanderbilt University, Nashville, Tennessee, USA

ARTICLE INFO

Keywords:

Rat, Rodent
Sample preparation
Contrast enhancing, Staining
Graded ethanol dehydration
Fixation
Stomach
Medical Images
Micro-CT

ABSTRACT

Background: Understanding stomach structure is crucial for studying gastrointestinal disorders, yet, existing studies are largely limited to two dimensional studies. Micro-CT offers high-resolution 3D imaging but requires contrast agents for soft tissues. This study investigates staining protocols and fixation durations to improve micro-CT imaging of rat stomachs, aiming to better visualize anatomy and facilitate structural understanding.

Method: Whole rat stomachs (n=13) were dissected, following euthanasia, and underwent a five-stage preparation process: fixation (2% neutral buffered formalin), dehydration (graded ethanol series), staining (0.75% alcoholic iodine and 2% alcoholic phosphotungstic acid), and imaged. Micro-CT scans were acquired with optimized parameters.

Results: PTA staining resulted in superior contrast and signal-to-noise ratio (SNR) compared to iodine staining. Fixation duration had minimal impact on image quality within the timeframe examined (3-17 weeks). Prolonged staining (over 14 weeks) resulted in tissue damage but improved fiber visibility. PTA staining caused significant tissue shrinkage (19% area reduction, 52% volume reduction)

Conclusion: PTA staining is recommended as a cost-effective, efficient stain for high-quality micro-CT of rat stomachs for gastric tissue structural studies.

1. Introduction

Gastrointestinal (GI) disorders related to the stomach and its sphincters (lower esophageal sphincter - LES, pyloric sphincter - PS) represent significant health challenges worldwide. Recent epidemiological data shows that conditions such as Gastroesophageal reflux disease (GERD), achalasia, bile reflux and pyloric stenosis, contribute to substantial morbidity rates [1–4]. Clinically, surgeries of LES (e.g. nissen fundoplication) and PS (e.g. gastric peroral endoscopic myotomy: G-POEM) have been shown to relieve significant symptoms associated

* Research supported in part by the Marsden Fund Council managed by Royal Society Te Apārangi.

* Corresponding author

** Principal corresponding author

 sabe848@aucklanduni.ac.nz (S. Wijenayaka); peng.du@auckland.ac.nz (P. Du)
ORCID(s): 0000-0002-5929-9794 (S. Wijenayaka)

with GERD and gastroparesis, respectively [5, 6]. However, despite the clinical significance, the detailed reconstruction of gastric tissue micro-structures remains a limiting factor in understanding how the whole stomach functions. While information can be extrapolated from microscopic evidences [7], there is a gap in envisaging how they vary spatially across the whole organ.

The stomach serves as the primary chamber for food breakdown in the human body. Here, both mechanical and biochemical processes contribute to transforming chewed food (bolus) particles into a smaller, more homogenous mixture. When bolus enters stomach, the LES acts as a one-way valve at the top of the stomach, preventing food and stomach acid from refluxing back into the esophagus. Contractions and slow waves of gastric wall originating in the upper stomach, propagate towards the pyloric valve, mixing food with gastric juices and propelling it towards the distal stomach (antrum) for further processing. The antrum, characterized by strong contractions, is responsible for the most intensive grinding and size reduction of food particles. Liquids and small particles can then pass through the pylorus into the duodenum, while larger indigestible components are temporarily returned to the stomach via retropulsion, which is facilitated by the functionality of PS. This repeated cycle of propulsion, grinding, and retropulsion ultimately reduces food particles and converts them into a mixture called chyme, which is subsequently released into the duodenum for further digestion [8].

The walls of these stomach areas are arranged in layers of different tissues, which not only facilitate the propagation of contractions and slow waves, but also regulate the opening and closing of the sphincter. Investigators have proposed that the evaluation of specific parameters, such as the muscle thickness, can serve as indicators for identifying LES and PS-related diseases [9, 10]. Moreover, muscle fiber architecture is a critical determinant of how muscular organs contract. Although cardiac studies have extensively investigated the role of fiber direction in heart function [11], very few studies conducted similar detailed analyses of the stomach. Understanding the layered structure of these sphincters is crucial in this context, as it consists of distinct regions, including the circular muscle (CM) layer, longitudinal muscle (LM) layer, and mucosa, which not only affect the absorption surface and mechanical functionality but also the electrical activity of the stomach. Existing studies typically limited analysis to two-dimensional

Micro-CT Imaging of *Ex-Vivo* Rat Stomachs

(2D) images, and primarily focus on gross anatomy or examine only specific areas of interest, overlooking the comprehensive understanding of muscle properties [7, 12–14]. Moreover, 2D-imaging methods suffer from potential loss of data as it requires slicing, deformation and/or flattening of the sample. In some cases, flattening the tissue might require corner pressure to avoid clapping back [7], potentially introducing stress artifacts.

Micro computed tomography (μ CT) offers the ability to image tissues at 1-5 μm resolutions in three-dimensions. Conventionally, the technique has been applied to distinguish structures with high contrast with the surrounding environment, such as mineralized tissues like bone and teeth. However, this limitation can be overcome by using a contrast enhancing agent, such as Lugol's solution and phosphotungstic acid (PTA), which facilitate demarcations between layers of soft tissue, enabling a more comprehensive analysis when imaged using μ CT. Although previous investigations have indeed imaged gastric tissues of various species using μ CT, due to the species size of the stomach, it was not possible to visualise the whole organ. Moreover, to the authors' knowledge, a comprehensive comparative analysis evaluating the impact of different staining agents and their optimal incubation times on μ CT imaging of gastric tissue has not been previously reported. Optimization of the staining protocol would significantly enhance image quality and highlight more intricate details of tissue structures thereby facilitating meaningful information extraction.

Rodents serve as valuable model organisms in biomedical research, and detailed anatomical information is essential for interpreting experimental findings to advance the knowledge of gastrointestinal physiology and pathology. Moreover, the small size of rodent stomach facilitates comprehensive three-dimensional visualization using μ CT in finer resolution, providing insights into its complex morphology. Previous histological studies have quantified the thickness of rat stomach muscle layers at specific fiducial points [7], often employing extrapolation techniques to estimate thickness across the entire organ [15]. These studies also described the fiber orientation of the LM and CM layers. The LM fibers were reported to exhibit a fingerprint-like pattern extending from the fundus to the antrum, while the CM fibers displayed a circumferential arrangement perpendicular to the LM.

Micro-CT Imaging of *Ex-Vivo* Rat Stomachs

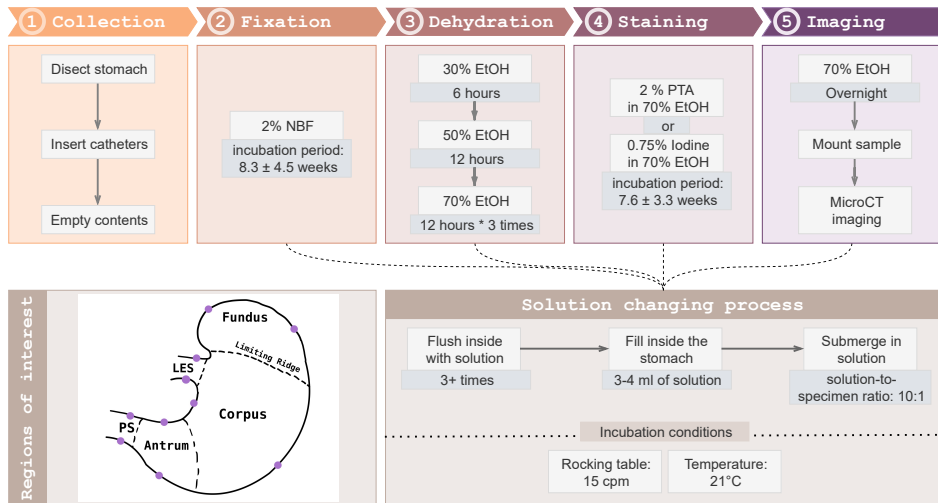


Figure 1: Methodology: Block 1-5 outline a concise overview of the sample preparation protocol followed in this study, along with their time durations for each individual step. Everytime solution is changed from one to another in those 5 steps, sequential procedure outlined in solution changing process is followed. Finally ten regions of interest (ROIs) were chosen for quality measurements (marked in purple), with 2 regions per each anatomical region in the stomach, ensuring coverage of both the lesser and greater curvature.

The present study investigates the effects of fixing period, staining agents and staining time on μ CT imaging of the whole rat stomach. We hypothesize that significant improvements in image quality and detailed structural features can be obtained while minimizing the preparation time of the tissue.

2. Methodology

The sample preparation and imaging protocol followed in this paper could be broken down into five key consecutive stages: collection, fixation, dehydration, staining, and imaging. These stages are outlined in Figure 1, along with their essential steps. Detailed discussions regarding each step and the rationale behind the chosen parameters are provided in the following sections (sections 2.1 to 2.5).

2.1. Specimen collection

Whole rat stomachs (n=13) were dissected following euthanasia approved by the University of Auckland Animal Ethics Committee (23005). To adhere to the 3Rs principle (replace, reduce, refine) and to maximize resource utilization, these stomachs were obtained from animals previously used in other *in-vivo* experiments. Dissection of the stomach should preserve at least 5 mm margin proximal to the LES and distal to the PS, to avoid damaging sphincter areas.

Following the dissection, introduce 2 mm outer diameter catheter through the LES and 3 mm outer diameter catheter through to the PS. The main purpose of the catheters was to allow better penetration of fixative and staining agents, as well as to maintain the sphincters in an "open" state. This immediate placement is crucial because these sphincter muscles naturally contract right after dissection.

Finally, proceed to remove all residuals inside the lumen by thoroughly flushing the inside of the stomach with water using a 5 ml syringe injected through the LES catheter, while keeping the PS catheter opened. Continue flushing until the water runs clear.

2.2. Fixation

The second stage of the process involves tissue fixation, which is essential to prevent post-mortem tissue degradation (autolysis). Fixation stabilizes the structural components of the tissue, ensuring their optimal preservation for subsequent processing steps.

Formalin is one of the most common fixatives used in histology and physiology studies. The 100% formalin solution is made by saturating water with 37-41% formaldehyde gas. Diluting a 100% formalin solution with water and Phosphate-Buffered Saline (PBS) creates Neutral Buffered Formalin (NBF). Generally, 10% NBF is considered the golden standard [16], but research in the GI tract show lower concentrations lesser than the 10% being used, while most of them use 3-4% [12, 17, 18]. In addition, lower concentrations were employed in μ CT studies of other rodent organs [19–22]. Selecting the optimal formalin concentration is critical for successful tissue fixation. Using a concentration that's too low can lead to inadequate fixation, while, excessively high concentrations can cause rapid fixation of the outer layers, increasing their density and preventing proper penetration of fixative into inner layers. This uneven fixation

Micro-CT Imaging of *Ex-Vivo* Rat Stomachs

can leave the inner layers under-fixed and susceptible to autolysis, thus compromise the quality of μ CT images.

In this study we used 2% NBF as the fixative and performed the solution handling process described in the figure 1. First, gently flush the specimen at least 3 times with 2% NBF. Then, fill the stomach with about 3-4 ml of the 2% NBF solution. The solution should distribute throughout the stomach, reaching the fundus without causing undue distension. Consequently, submerge the entire dissected stomach sample, including the catheters, in a container filled with fresh 2% NBF. Maintaining a sufficient solution-to-specimen ratio is essential in this step. While some studies suggest a 5:1 ratio for larger samples due to practical difficulties [23], typically a solution-to-specimen ratio less than 10:1 is considered inadequate for fixation [16, 24, 25]. Although a 10:1 ratio remains the established standard, based on the findings of Buesa and Peshkov (2012) it can be argued that the 2:1 ratio is sufficient [26]. However, following the most prevalent practice, this study adopted a 10:1 solution-to-specimen ratio for optimal tissue preservation. To conclude the fixation process, place the submerged specimen on a rocking table set to 15 cycles per minute at room temperature (21°C).

Solution's pH level plays a significant role in fixation process. When using formalin, frequent replacement with fresh solution is recommended to maintain a stable pH range. This is because formalin naturally acidifies over time. NBF, on the other hand, utilizes PBS to maintain a neutral pH (typically between 7.2-7.4 pH [16]). This consistent pH level facilitates optimal fixative penetration into the tissue and prevents polymerization [25]. Our experiments indicate that the pH of 2% NBF remains relatively stable around 7.2 pH, hence we did not proceed with any replacement.

When it comes to fixation duration, sample depth (or thickness in our case) plays a crucial role. Fixation depth (d) is considered proportional to the square root of fixation time (t); $d = k\sqrt{t}$ [16]. The constant k depends on the fixative. For instance, 0.79 for 10% NBF, which can penetrate roughly 1 mm per hour. Given the variable thickness 1-3 mm of our samples, a fixation duration of 15 hours should ensure adequate penetration throughout the tissue. However, this study explored the influence of fixation duration on specimen's imaging

quality by employing a range of incubation periods (8.3 weeks \pm 4.5 weeks). The findings related to fixation duration are presented in the results (section 3).

2.3. Dehydration

The dehydration step is performed to remove water molecules from the fixed sample. Incomplete dehydration can compromise μ CT imaging in several ways. First, trapped water molecules within the tissue can hinder the penetration of staining agents, leading to inadequate staining and compromised visualization of different structures [27]. Second, water loss during long μ CT scans can cause subtle movements in the sample. These movements can introduce artifacts and blur the final image [28]. Finally, while not relevant to this study, residual water can interfere with the embedding process if the medium is hydrophobic [29].

A variety of dehydration techniques exist for sample preparation in histology, microscopy, and X-ray imaging. These include critical-point drying (CPD), alcohol dehydration, air drying, and novel methods like EOS (evaporation-of-organic-solvent). CPD, which replaces water with CO₂, is regarded as best for preserving fine structures and achieving high signal-to-noise (SNR) ratios [30]. However, it is time-consuming and expensive [31]. While chemical drying with hexamethyldisilazane (HMDS) offers good results [31], it can cause excessive tissue shrinkage and damage [30]. Air drying and the EOS technique, though less frequently reported in literature, have also demonstrated success in computed tomography by enhancing contrast between muscle layers [30, 32, 33].

Alcohol dehydration, particularly with ethanol (EtOH), is the most common drying technique in histology due to its miscibility with water, hardening effect, strong dehydration capacity, and tissue penetration [34, 35]. As demonstrated by Dudak et al. (2016) [36], using only 50% ethanol maintained the tissue's natural appearance but lacked sufficient contrast, while directly applying 97% ethanol caused severe deformation and ruptures. Whereas, a graded ethanol series balanced tissue preservation and contrast enhancement. A gradually increasing ethanol concentration, preventing rapid water loss and protecting delicate structures during dehydration [34]. Appendix A summarizes various graded ethanol series used in previous studies. It indicates that the choice of specific concentrations and incubation times appears

to be based on individual researcher preferences. While a general range of $30 \pm 5\%$ to $70 \pm 5\%$ ethanol with a three-fold concentration increase seems common, incubation times vary widely, ranging from hours to days or even weeks. This discrepancy likely reflects the influence of tissue size and characteristics on the dehydration process. However, researchers generally follow either a gradual increase in incubation time with increasing ethanol concentration or a constant incubation time throughout the series.

This protocol utilizes graded ethanol dehydration process starting from 30% concentration and gradually increasing to 70%. The specific ethanol concentrations and corresponding incubation times are detailed in figure 1. Transferring the specimen from one solution to another followed the same standardized protocol as the fixative (outlined in figure 1: solution changing process). For instance, when transitioning from 30% EtOH to 50% EtOH, the specimen was first flushed with 50% EtOH at least three times. Subsequently, the stomach cavity was filled with the 50% EtOH and completely submerged in the fresh solution.

2.4. Staining (contrast enhancing)

Following dehydration, the next step involves contrast enhancement or staining of the sample. Soft tissues, like muscles or organ walls, generally have a lower mineral content compared to hard tissues like bones and teeth. This lower mineral content translates to a smaller difference in X-ray attenuation between soft tissues. Hence, the contrast between different soft tissues in a μ CT scan is often weak, making it difficult to distinguish their boundaries and define their 3D morphology. Contrast agents like Lugol's solution address this by selectively accumulating in specific soft tissues. These agents contain elements like Iodine that strongly attenuate X-rays, essentially making the target tissues brighter in the μ CT scan.

There are two main types of contrast agents commonly used in μ CT: Iodine-based stains and phosphotungstic acid (PTA) [37]. Both stains offer advantages in terms of simplicity and robustness of the staining procedures. The staining times were found to be flexible, as long as sufficient time is allowed for the stain to penetrate the tissues [37].

Iodine based stains readily diffuses into fixed tissues due to its small molecule size. Alcoholic or aqueous solutions of iodine can typically stain most specimens within a few hours,

although long incubation periods are generally observed [21, 22, 38]. However, inter-tissue discrimination is more challenging when employing Iodine since various tissues tend to stain at similar levels [39] resulting in fuzzy reconstructions and random groupings in a few areas of the tissue [32]. In contrast to iodine, PTA has a known affinity for binding to various proteins and connective tissues which help in better soft-tissue contrast. However, some studies have reported that PTA's high radiopacity could mask subtle structural details, making it difficult to distinguish boundaries like those of blood vessels [40, 41]. Moreover, since PTA has much larger molecules, it requires longer incubation time [37].

Since existing research suggests Iodine and PTA offer comparable advantages for various staining aspects, this study employed both contrast agents to ensure achieving the highest possible image quality. Specifically, it utilized 0.75% alcoholic I_2KI solution and 2% alcoholic PTA. Details of the solution preparation is outlined in appendix B and the solution changing process remains identical to the previously described steps. Similar to fixation, this study explored the influence of staining duration by employing a range of incubation times (7.6 weeks \pm 3.3 weeks). For extended staining durations, replacing the stain solution every two weeks is recommended [42, 43].

2.5. Sample mounting and imaging

Prior to μ CT imaging, the sample is transferred to a 70% EtOH solution for overnight incubation. This step facilitates the removal of unbound staining agents, thereby enhancing image quality by minimizing background noise [22, 38].

Previous research has explored various sample mounting techniques, including embedding in wax [12, 17] or agarose gel [42–44] and submersion in ethanol [38, 44]. In contrast, this study utilizes a simpler approach: the sample is positioned between two 120 μ m transparent styrene pieces and enclosed within a plastic tube containing enough ethanol in the bottom of the tube to prevent sample from dehydration, mirroring the technique described in De Souza E Silva et al. (2017) [45]. The tube was subsequently sealed with a polystyrene lid and an additional foil layer on top of it to prevent evaporation.

Micro-CT Imaging of *Ex-Vivo* Rat Stomachs

	Parameter	Values (mean \pm sd)
Imaging	Source Voltage (kV)	100
	Source Current (uA)	100
	Image Rotation	0.15
	Number of connected scans	3
	Image Pixel Size (μm)	8.69 \pm 1.0
	Object to Source (mm)	103.87 \pm 11.89
	Camera to Source (mm)	215.23
	Exposure (ms)	681.44 \pm 228.57
	Rotation Step (deg)	0.34 \pm 0.05
	Frame Averaging	2.56 \pm 0.53
	Random Movement	3.78 \pm 0.67
	Scan duration (HH:MM:SS)	07:08:56 \pm 01:34:59
	Median Filtering	On
Reconstruction	Flat Field Correction	On
	Type Of Motion	Step and shoot
	Postalignment Applied	1
	Total reconstruction time (HH:MM:SS)	00:12:45 \pm 00:05:03
Reconstruction	Pixel Size (μm)	8.69 \pm 0.99
	Smoothing kernel	Gaussian
	Smoothing	2.89 \pm 0.33
	Reconstruction convolution filter	Hamming ($\alpha=0.54$)
	Ring Artifact Correction	11.89 \pm 10.36
	Undersampling factor	1
	Beam Hardening Correction (%)	79.44 \pm 17.64

Table 1

Acquisition and reconstruction parameters for stained scans, summarized using all 13 scans.

The sample is subsequently positioned within a SkyScan 1172 micro-CT scanner (Bruker, Billerica, MA, USA) for the image acquisition. A 0.25 mm aluminum filter is placed between the X-ray source and the sample to induce beam hardening. The reconstructed images were then processed using NRecon software (Bruker, Billerica, MA, USA) for noise reduction and artifact removal. Extensive list of parameters for image acquisition and reconstruction is given in table 1.

2.6. Quantification of quality in μCT scans

In image-based structural analysis, quality of the μCT scans plays a crucial role. While it is largely influenced by the specimen preparation process, it could also be influenced by the scanner based characteristics and image acquisition parameters. Given that this study utilized the same μCT scanner and maintained a fairly similar set of parameters, variations in specimen preparation are likely to have the most significant impact on image quality.

Two key factors that influence image quality are signal-to-noise ratio (SNR) and contrast-to-noise ratio (CNR). SNR refers to the strength of the desired signal, representing the anatomical structures of interest, compared to the background noise inherent in the image. A higher SNR translates to a clearer image with better visibility of the structures whereas lower SNR will present with a grainy image. CNR builds upon SNR by considering the difference in signal intensity between the structures of interest, in this case muscle and mucosa. Even with a good SNR, structures with similar signal intensities can blend together, making them difficult to distinguish. CNR helps quantify this contrast, with a higher value indicating a clearer distinction between the target structures.

To quantify the SNR and CNR, this study considered 10 regions of interests (ROIs), from 5 different anatomical regions as depicted in figure 1. The SNR was calculated for each ROI within each tissue type. The calculation adopted the concepts from Ferrand et al. (2019) [46], which defines SNR as the ratio between the mean signal intensity (\bar{x}) and the standard deviation (s) of the signal within a specific ROI. Subsequently, the SNR for the entire experiment (SNR_{exp}) was determined by averaging the SNR values obtained for all individual ROIs across both tissue types (equation (1)). Here, N is the total number of ROIs for both tissue types which is 20 (2×10) in our case.

$$SNR = \frac{\bar{x}}{s}$$

$$SNR_{exp} = \frac{1}{N} \times \sum_{i=1}^{N=20} SNR_i \quad (1)$$

Building upon the SNR analysis, the CNR was also calculated using \bar{x} and s . As described by Isherwood et al. (2021) [47], equation (2) was employed to determine the CNR for each ROI, considering two tissue types within that region. Subsequently, the CNR values for all ROIs across the experiments were averaged to obtain a representative overall CNR for the experiment.

Micro-CT Imaging of *Ex-Vivo* Rat Stomachs

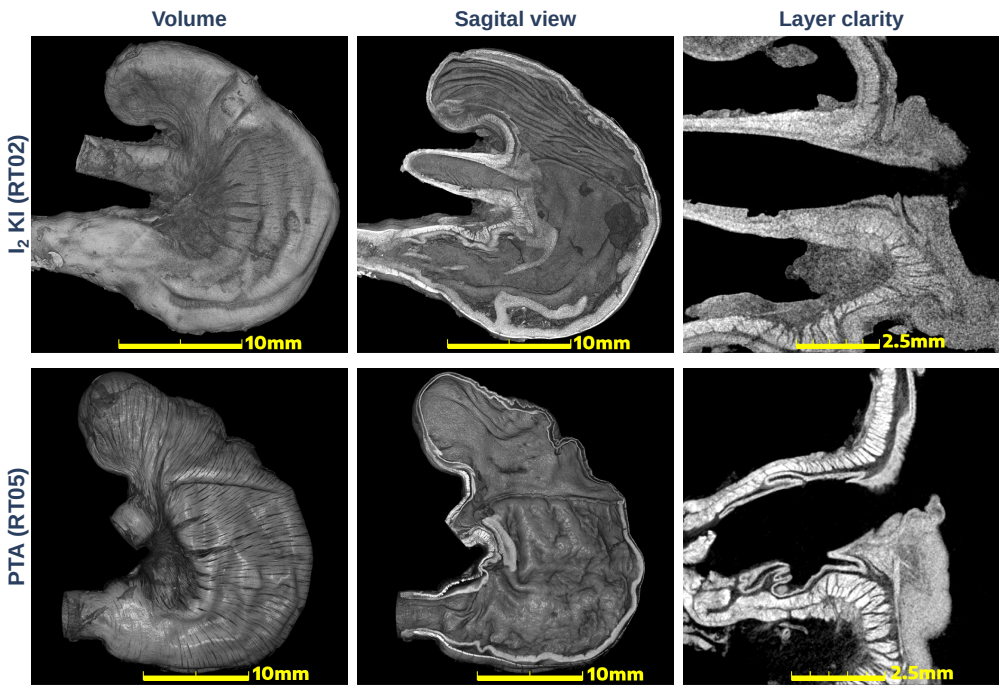


Figure 2: Visual comparison of stain effectiveness using two samples from each stain: Volume view shows a prominent fiber direction in the PTA samples. Cross-sectional images allow comparison of muscle and mucosal layer visibility following staining with each contrast agent. Zoomed in images provide a better comparison of the layer clarity and noise level observed around LES for each stain.

$$CNR_{roi} = \frac{|\bar{x}_{muscle} - \bar{x}_{mucosa}|}{\sqrt{s_{muscle}^2 + s_{mucosa}^2}} \quad (2)$$

$$CNR_{exp} = \frac{1}{N} \times \sum_{i=1}^{N=10} CNR_i$$

To ensure a statistically robust comparison of the staining techniques in figure 3, we randomly sampled the PTA-stained SNR values such that number of data points for both stains are equal.

3. Results

To assess the impact of these staining methods, this research employed a comprehensive approach involving visual inspection and quantitative analysis.

Micro-CT Imaging of *Ex-Vivo* Rat Stomachs

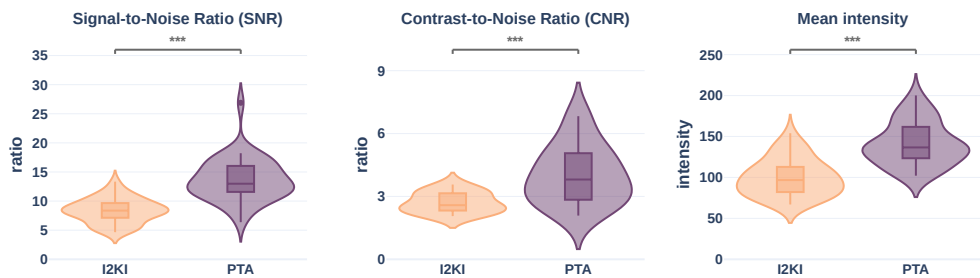


Figure 3: Quantitative comparison of stains ($\alpha=0.05$): The graph was drawn considering 20 random samples from PTA against all Iodine-based samples to preserve equality in number of samples. All three measurements considered in the study performed better in PTA stained experiments.

Figure 2 shows a visual comparison of two experiments done under two stains side-by-side. It revealed superior tissue layer definition in the PTA-stained sample compared to I₂KI-stained sample. Notably, the PTA-stained sample exhibits a clear demarcation between the circumferential and longitudinal muscle layers, particularly evident in the close-up images of the LES. Moreover, I₂KI-stained sample appears grainier compared to its counterpart, presenting lower image clarity, characterized by increased noise and a potentially lower SNR. Additionally, the PTA stain managed to effectively highlighted the directional orientation of tissue fibers.

Quantitative comparison of SNR, CNR and mean intensity, supported by Welch's unequal variances t-test, revealed statistically significant differences between the iodine and PTA staining groups ($p < 0.0005$ for all metrics) [figure 3]. PTA consistently outperformed iodine across all evaluated parameters, proving the visual observations presented in figure 2.

To identify regions with optimal contrast between tissue layers, regional SNRs were analyzed considering only PTA-stained samples [figure 4]. Statistically significant differences in SNR between tissue layers were found in ROIs labelled GC_Fundus1 ($p=0.005$), GC_Pyloric ($p=0.012$), LC_Corpus ($p=0.045$), LC_LES ($p=0.045$). Both LC_Corpus and LC_LES are marginal in statistical significance. However, these regions with significant SNR differences are not spatially in close proximity, with the exception of the LC_corpus and LC_LES. Further investigation into CNR of regions considering only PTA-stained samples, demonstrated a lack

Micro-CT Imaging of *Ex-Vivo* Rat Stomachs

of significant contrast differentiation between the two tissue layers across all regions ($p = 0.075$), supporting the lack of SNR difference by region.

The influence of fixation and stain duration on these measurements are visualized in figure 5. Our findings suggest that fixation time has a minimal impact on SNR and CNR within the examined timeframe, while some immunohistochemical studies suggests a correlation between prolonged fixation and the requirement for extended staining durations due to potential tissue hardening and reduced stain penetration [48]. This is evidenced by the statistically similar SNR and CNR values obtained for samples RT04, RT12, and RT13, which has almost similar staining time (7.2, 7.8 and 8 weeks respectively), yet 14 weeks difference (2.9, 16.7 and 16.5 weeks) in fixing time. To optimize the fixation process, a duration of three weeks is sufficient. However, our findings indicate flexibility in this timeframe, with acceptable results observed within a range of three to seventeen weeks.

With respect to staining, prolonged staining durations (exceeding approximately fourteen weeks) can lead to tissue damage, as evidenced by tissue tearing in samples marked in red in figure 5. This is likely attributed to the dehydrating effects of the alcoholic staining solution. Samples with staining durations between seven and nine weeks demonstrated optimal results in

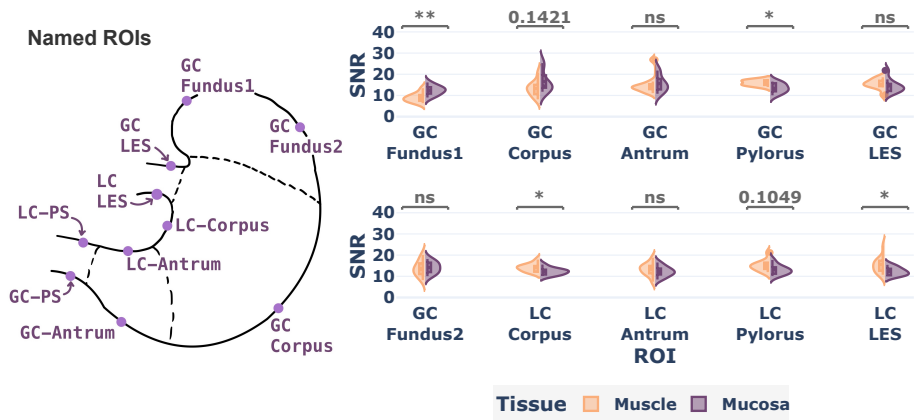


Figure 4: SNR comparison between PTA-stained tissue layers of different regions ($\alpha=0.05$): Regions named GC_Fundus1 ($p=0.005$), GC_Pyloric ($p=0.012$), LC_Corpus ($p=0.045$), and LC_LES ($p=0.045$) showed a statistical significance. Except for latter two regions that are marginal, these regions are not in close proximity.

Micro-CT Imaging of *Ex-Vivo* Rat Stomachs

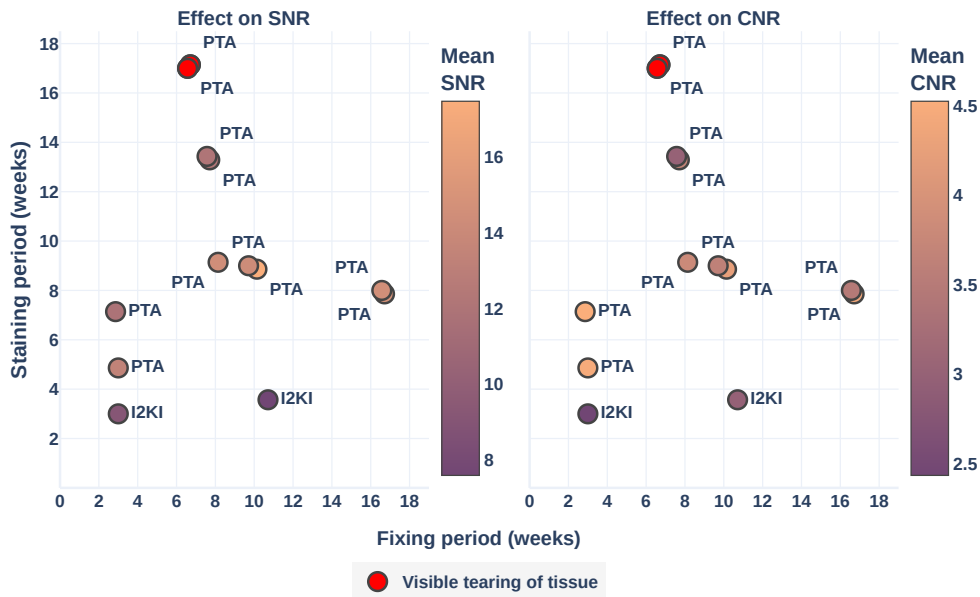


Figure 5: Staining and fixing time contribution to quality measurements: The fixative time does not seem to contribute to the quality of imaging while excessive staining times contribute to visible tissue tearing. The staining duration between seven and nine weeks display a better quality irrespective of fixation duration.

terms of SNR and CNR. Specifically, three out of the top five performing samples based on CNR and all of the top five samples based on SNR fell within this staining duration range. However, it is worth noting that samples with longer staining durations had enhanced fiber orientation visibility, hence introduced increased variability in signal intensity measurements, as evidenced by their higher standard deviations. This could primarily attributed to the pronounced fiber orientation within the tissue, rather than noise fluctuations. This variability consequently affected the calculated SNR and CNR values as described in equations 1 and 2. To mitigate this effect, obtaining samples with minimal fiber orientation from ROIs were prioritized during initial mean intensity calculations. However, completely eliminating the influence of fiber orientation proved challenging.

In addition, analysis of PTA-stained samples revealed significant shrinkage, with a mean reduction in area of $19.06 \pm 9.87\%$ and a volume reduction of $51.56 \pm 5.75\%$. This phenomenon could be attributed to the dehydrating properties of the alcoholic staining medium, which

extracts water from the tissue. While not linear, given the relationship between staining duration and dehydration, it is anticipated that prolonged exposure to the staining solution would further amplify this effect.

4. Discussion

The present study aimed to investigate the impact of staining protocols and fixation durations on micro-CT imaging quality for rat stomachs. Our findings demonstrate the superior performance of PTA staining over iodine-based staining in terms of image clarity, tissue contrast, and fiber orientation. The conclusions drawn are based on a combination of visual inspection and quantitative quality analysis. These findings highlight the importance of stain selection in optimizing micro-CT image quality for detailed tissue analysis.

Regional variations in SNR and CNR within PTA-stained samples were also explored. However, the lack of substantial statistical significance in both measures are observed between regions, indicating the applied staining protocol yielded almost uniform staining across the entire organ, despite the modest tissue thickness differences observed in the fundus when compared to other regions.

The findings regarding optimal fixation and staining durations provide valuable guidelines for future studies. Our results indicate that while extended fixation durations (up to 17 weeks) did not significantly compromise image quality, prolonged staining times (exceeding approximately fourteen weeks) can lead to tissue damage. Moreover, staining period larger than nine weeks increased image variability, due to prominent fiber bundles. Based on our findings, a fixation duration of three weeks coupled with a staining period between seven and nine weeks is optimal for comprehensive analyses of the anatomical structure, including assessments of layer thickness and fiber orientation. However, give consideration to tissue shrinkage when reporting structural data obtained from such PTA-stained samples, as it is substantial according to our observations. Nevertheless, if the primary focus is on fiber orientation, extending the staining period to fourteen weeks may enhance fiber visibility, without compromising tissue integrity, as observed in our study.

5. Conclusion

Our findings demonstrate the superiority of PTA staining over iodine-based staining in terms of image quality, which is supported by both visual assessment and quantitative metrics (SNR and CNR). A fixation period of approximately three weeks, coupled with a staining duration between seven and nine weeks, provides an optimal balance between image quality and tissue preservation. This protocol will inform our future work related to image segmentation and quantitative analysis of the stomach, LES, and PS muscle layers, which will allow for a better understanding of how these anatomical structures relate to gastric functions.

Building upon the findings of this study, future research could focus on further optimizing staining protocols and exploring alternative staining agents to potentially mitigate the observed tissue shrinkage and variability attributed to fiber orientation. Additionally, investigating the impact of different fixation methods, such as perfusion fixation, on image quality would be beneficial. A more comprehensive analysis of the relationship between tissue thickness and image quality could also provide valuable insights for future studies. Furthermore, applying these optimized imaging protocols to a larger sample size would enhance the statistical power of the study and enable more robust conclusions.

References

- [1] A. J. Gawron, D. D. French, J. E. Pandolfino, and C. W. Howden, “Economic Evaluations of Gastroesophageal Reflux Disease Medical Management: A Systematic Review,” *PharmacoEconomics*, vol. 32, no. 8, p. 745, 2014.
- [2] D. C. Sadowski, F. Ackah, B. Jiang, and L. W. Svenson, “Achalasia: incidence, prevalence and survival. A population-based study,” *Neurogastroenterology and motility : the official journal of the European Gastrointestinal Motility Society*, vol. 22, 9 2010.
- [3] K. Donda, B. Asare-Afriyie, M. Ayensu, M. Sharma, J. K. Amponsah, P. Bhatt, M. A. Hesse, and F. Dapaah-Siakwan, “Pyloric Stenosis: National Trends in the Incidence Rate and Resource Use in the United States From 2012 to 2016,” *Hospital pediatrics*, vol. 9, pp. 923–932, 12 2019.
- [4] K. H. Boulton and P. W. Dettmar, “A narrative review of the prevalence of gastroesophageal reflux disease (GERD),” *Annals of Esophagus*, vol. 5, 3 2022.
- [5] J. E. Richter, A. Kumar, S. Lipka, B. Miladinovic, and V. Velanovich, “Efficacy of Laparoscopic Nissen Fundoplication vs Transoral Incisionless Fundoplication or Proton Pump Inhibitors in Patients With Gastroesophageal

Micro-CT Imaging of *Ex-Vivo* Rat Stomachs

- Reflux Disease: A Systematic Review and Network Meta-analysis," *Gastroenterology*, vol. 154, pp. 1298–1308, 4 2018.
- [6] J. Xu, T. Chen, S. Elkholy, M. Xu, Y. Zhong, Y. Zhang, W. Chen, W. Qin, M. Cai, and P. Zhou, "Gastric Peroral Endoscopic Myotomy (G-POEM) as a Treatment for Refractory Gastroparesis: Long-Term Outcomes," *Canadian Journal of Gastroenterology and Hepatology*, vol. 2018, p. 6409698, 1 2018.
- [7] M. R. Di Natale, L. Patten, J. C. Molero, M. J. Stebbing, B. Hunne, X. Wang, Z. Liu, and J. B. Furness, "Organisation of the musculature of the rat stomach," *Journal of Anatomy*, vol. 240, pp. 711–723, 4 2022.
- [8] F. Kong and R. P. Singh, "A Human Gastric Simulator (HGS) to Study Food Digestion in Human Stomach," *Journal of Food Science*, vol. 75, pp. E627–E635, 11 2010.
- [9] M. J. Siegel and E. Y. Lee, "Paediatric bowel and mesentery," in *Clinical Ultrasound*, vol. 2-2, pp. 1383–1405, Elsevier, 1 2011.
- [10] I. Dogan, J. L. Puckett, B. S. Padda, and R. K. Mittal, "Prevalence of increased esophageal muscle thickness in patients with esophageal symptoms," *The American journal of gastroenterology*, vol. 102, pp. 137–145, 1 2007.
- [11] C. Papadacci, V. Finel, J. Provost, O. Villemain, P. Bruneval, J. L. Gennisson, M. Tanter, M. Fink, and M. Pernot, "Imaging the dynamics of cardiac fiber orientation in vivo using 3D Ultrasound Backscatter Tensor Imaging," *Scientific Reports 2017 7:1*, vol. 7, pp. 1–9, 4 2017.
- [12] R. Yassi, L. K. Cheng, S. Al-Ali, G. Sands, D. Gerneke, I. LeGrice, A. J. Pullan, and J. A. Windsor, "Three-dimensional high-resolution reconstruction of the human gastro-oesophageal junction," *Clinical anatomy (New York, N.Y.)*, vol. 23, pp. 287–96, 4 2010.
- [13] A. Garrett, N. Rakhilin, N. Wang, M. Boguñá, S. Pajevic, P. J. Bassar, D. Liao, H. Gregersen, P. Agger, C. Laustsen, S. Ringgaard, H. Stødkilde-Jørgensen, and J. Zhao, "3D reconstruction and fiber quantification in the pig lower esophageal sphincter region using in vitro diffusion tensor imaging," *Biomedical Physics & Engineering Express*, vol. 4, p. 025002, 1 2018.
- [14] M.-S. Hur, S. Lee, T. M. Kang, and C.-S. Oh, "The three muscle layers in the pyloric sphincter and their possible function during antropyloroduodenal motility," *Scientific Reports*, vol. 11, p. 20094, 10 2021.
- [15] R. Avci, J. D. Wickens, M. Sangi, O. N. Athavale, M. R. Di Natale, J. B. Furness, P. Du, and L. K. Cheng, "A Computational Model of Biophysical Properties of the Rat Stomach Informed by Comprehensive Analysis of Muscle Anatomy," *Annual International Conference of the IEEE Engineering in Medicine and Biology Society. IEEE Engineering in Medicine and Biology Society. Annual International Conference*, vol. 2022, pp. 4954–4957, 2022.
- [16] C. Layton, J. D. Bancroft, and S. K. Suvarna, "Fixation of tissues," in *Bancroft's Theory and Practice of Histological Techniques*, ch. 4, pp. 40–63, Netherlands: Elsevier, 2019.
- [17] A. K. Vegesna, J. A. Sloan, B. Singh, S. J. Phillips, A. S. Braverman, M. F. Barbe, M. R. Ruggieri, and L. S. Miller, "Characterization of the Distal Esophagus High-Pressure Zone with Manometry, Ultrasound

Micro-CT Imaging of Ex-Vivo Rat Stomachs

- and Micro-Computed Tomography," *Neurogastroenterology and motility : the official journal of the European Gastrointestinal Motility Society*, vol. 25, p. 53, 1 2013.
- [18] D. Liao, H. Gregersen, P. Agger, C. Laustsen, S. Ringgaard, H. Stødkilde-Jørgensen, and J. Zhao, "3D reconstruction and fiber quantification in the pig lower esophageal sphincter region using in vitro diffusion tensor imaging," *Biomedical Physics & Engineering Express*, vol. 4, p. 025002, 1 2018.
- [19] K. C. Chen, A. Arad, Z. M. Song, and D. Croaker, "High-definition neural visualization of rodent brain using micro-CT scanning and non-local-means processing," *BMC Medical Imaging*, vol. 18, pp. 1–13, 10 2018.
- [20] I. Hammoura, R. H. Fiechter, S. H. Bryant, S. Westmoreland, G. Kingsbury, W. Waegell, S. W. Tas, D. L. Baeten, M. G. van de Sande, M. N. van Tok, and L. M. van Duivenvoorde, "Dual Blockade of TNF and IL-17A Inhibits Inflammation and Structural Damage in a Rat Model of Spondyloarthritis," *International Journal of Molecular Sciences*, vol. 23, 1 2022.
- [21] P. Heimel, N. V. Swiadek, P. Slezak, M. Kerbl, C. Schneider, S. Nürnberg, H. Redl, A. H. Teuschl, and D. Hercher, "Iodine-Enhanced Micro-CT Imaging of Soft Tissue on the Example of Peripheral Nerve Regeneration," *Contrast Media & Molecular Imaging*, vol. 2019, pp. 1–15, 3 2019.
- [22] A. Doost, A. Rangel, Q. Nguyen, G. Morahan, and L. Arnolda, "Micro-CT scan with virtual dissection of left ventricle is a non-destructive, reproducible alternative to dissection and weighing for left ventricular size," *Scientific Reports 2020 10:1*, vol. 10, pp. 1–9, 8 2020.
- [23] E. A. Sampedro-Carrillo, "Sample Preparation and Fixation for Histology and Pathology," in *Methods in Molecular Biology*, vol. 2422, pp. 33–45, New York, NY: Humana, 2022.
- [24] A. Scarano, G. Iezzi, and A. Piattelli, "Common Fixatives In Hard-Tissue Histology," in *Handbook of Histology Methods for Bone and Cartilage* (Y. H. An and K. L. Martin, eds.), ch. 9, pp. 159–165, Totowa, NJ: Humana Press, 2003.
- [25] R. Thavarajah, V. Mudimbaimannar, J. Elizabeth, U. Rao, and K. Ranganathan, "Chemical and physical basics of routine formaldehyde fixation," *Journal of Oral and Maxillofacial Pathology*, vol. 16, p. 400, 9 2012.
- [26] R. J. Buesa and M. V. Peshkov, "How much formalin is enough to fix tissues?," *Annals of Diagnostic Pathology*, vol. 16, pp. 202–209, 6 2012.
- [27] S. Jimson, L. Malathi, G. Kumar, and N. Balachander, "Artifact in Histological Section," *Biomedical and Pharmacology Journal*, vol. 9, pp. 843–845, 8 2016.
- [28] A. du Plessis, C. Broeckhoven, A. Guelpa, and S. G. le Roux, "Laboratory x-ray micro-computed tomography: a user guideline for biological samples," *GigaScience*, vol. 6, pp. 1–11, 6 2017.
- [29] S. Eminaga, P. Teekakirikul, C. E. Seidman, and J. G. Seidman, "Detection of markers of cell proliferation by immunofluorescent staining and microscopy imaging in paraffin-embedded tissue sections," *Current protocols in molecular biology*, vol. 115, p. 14.25.1, 7 2016.

Micro-CT Imaging of *Ex-Vivo* Rat Stomachs

- [30] Y. Gutiérrez, D. Ott, M. Töpperwien, T. Salditt, and C. Scherber, “X-ray computed tomography and its potential in ecological research: A review of studies and optimization of specimen preparation,” *Ecology and Evolution*, vol. 8, p. 7717, 8 2018.
- [31] F. Friedrich, Y. Matsumura, H. Pohl, M. Bai, T. Hörschemeyer, and R. G. Beutel, “Insect morphology in the age of phylogenomics: innovative techniques and its future role in systematics,” *Entomological Science*, vol. 17, pp. 1–24, 1 2014.
- [32] M. Reichardt, M. Töpperwien, A. Khan, F. Alves, and T. Salditt, “Fiber orientation in a whole mouse heart reconstructed by laboratory phase-contrast micro-CT,” *Journal of Medical Imaging*, vol. 7, p. 1, 3 2020.
- [33] M. Töpperwien, M. Krenkel, D. Vincenz, F. Stöber, A. M. Oelschlegel, J. Goldschmidt, and T. Salditt, “Three-dimensional mouse brain cytoarchitecture revealed by laboratory-based x-ray phase-contrast tomography,” *Scientific Reports*, vol. 7, p. 42847, 2 2017.
- [34] M. Lai and B. Lü, “Tissue Preparation for Microscopy and Histology,” *Comprehensive Sampling and Sample Preparation: Analytical Techniques for Scientists*, pp. 53–93, 1 2012.
- [35] A. M. Glauert and P. R. Lewis, “Dehydration methods,” in *Biological Specimen Preparation for Transmission Electron Microscopy*, ch. 4, pp. 129–146, Princeton, NJ: Princeton University Press, 12 1998.
- [36] J. Dudak, J. Zemlicka, J. Karch, M. Patzelt, J. Mrzilkova, P. Zach, Z. Hermanova, J. Kvacek, and F. Krejci, “High-contrast X-ray micro-radiography and micro-CT of ex-vivo soft tissue murine organs utilizing ethanol fixation and large area photon-counting detector,” *Scientific Reports 2016 6:1*, vol. 6, pp. 1–9, 7 2016.
- [37] B. D. Metscher, “Micro CT for comparative morphology: Simple staining methods allow high-contrast 3D imaging of diverse non-mineralized animal tissues,” *BMC Physiology*, vol. 9, pp. 1–14, 6 2009.
- [38] J. M. d. S. e. Silva, I. Zanette, P. B. Noël, M. B. Cardoso, M. A. Kimm, and F. Pfeiffer, “Three-dimensional non-destructive soft-tissue visualization with X-ray staining micro-tomography,” *Scientific Reports*, vol. 5, p. 14088, 9 2015.
- [39] P. Swart, M. Wicklein, D. Sykes, F. Ahmed, and H. G. Krapp, “A quantitative comparison of micro-CT preparations in Dipteron flies,” *Scientific Reports 2016 6:1*, vol. 6, pp. 1–12, 12 2016.
- [40] K.-C. Chen, A. Arad, Z.-M. Song, and D. Croaker, “High-Definition Heart Visualization using Micro-CT Scanning on Experimental Rats,” 2018.
- [41] A. Doost and L. Arnolda, “Iodine staining outperforms phosphotungstic acid in high-resolution micro-CT scanning of post-natal mice cardiac structures,” <https://doi.org/10.11117/I.JMI.8.2.027001>, vol. 8, p. 027001, 3 2021.
- [42] M. Kaucka, T. Zikmund, M. Tesarova, D. Gyllborg, A. Hellander, J. Jaros, J. Kaiser, J. Petersen, B. Szarowska, P. T. Newton, V. Dyachuk, L. Li, H. Qian, A. S. Johansson, Y. Mishina, J. D. Currie, E. M. Tanaka, A. Erickson, A. Dudley, H. Brismar, P. Southam, E. Coen, M. Chen, L. S. Weinstein, A. Hampl, E. Arenas, A. S. Chagin, K. Fried, and I. Adameyko, “Oriented clonal cell dynamics enables accurate growth and shaping of vertebrate

Micro-CT Imaging of *Ex-Vivo* Rat Stomachs

- cartilage,” *eLife*, vol. 6, 4 2017.
- [43] M. Tesařová, T. Zikmund, M. Kaucká, I. Adameyko, J. Jaroš, D. Paloušek, D. Škaroupka, and J. Kaiser, “Use of micro computed-tomography and 3D printing for reverse engineering of mouse embryo nasal capsule,” *Journal of Instrumentation*, vol. 11, p. C03006, 3 2016.
- [44] J. Missbach-Guentner, D. Pinkert-Leetsch, C. Dullin, R. Ufartes, D. Hornung, B. Tampe, M. Zeisberg, and F. Alves, “3D virtual histology of murine kidneys –high resolution visualization of pathological alterations by micro computed tomography,” *Scientific Reports 2018 8:1*, vol. 8, pp. 1–14, 1 2018.
- [45] J. Martins De Souza E Silva, J. Utsch, M. A. Kimm, S. Allner, M. F. Epple, K. Achterhold, and F. Pfeiffer, “Dual-energy micro-CT for quantifying the time-course and staining characteristics of ex-vivo animal organs treated with iodine- and gadolinium-based contrast agents,” *Scientific Reports 2017 7:1*, vol. 7, pp. 1–10, 12 2017.
- [46] A. Ferrand, K. D. Schleicher, N. Ehrenfeuchter, W. Heusermann, and O. Biehlmaier, “Using the NoiSee workflow to measure signal-to-noise ratios of confocal microscopes,” *bioRxiv*, p. 291500, 12 2018.
- [47] S. J. S. Isherwood, P. L. Bazin, A. Alkemade, and B. U. Forstmann, “Quantity and quality: Normative open-access neuroimaging databases,” *PLOS ONE*, vol. 16, p. e0248341, 3 2021.
- [48] J. Lenz, D. Macháčová, P. Konečná, L. Fiala, M. Kyllar, and F. Tichý, “Effects of different fixatives over different fixation times, including Antigenfix, on immunohistochemical studies,”
- [49] O. Jehoon, H. J. Kwon, T. H. Cho, S. H. Woo, Y. H. Rhee, and H. M. Yang, “Micro-computed tomography with contrast enhancement: An excellent technique for soft tissue examination in humans,” *PLOS ONE*, vol. 16, p. e0254264, 7 2021.

Micro-CT Imaging of *Ex-Vivo* Rat Stomachs

Ref	Animal	Organ	Ethanol (%)	Dehydration time	Stain	Stain time
[38]	Rodent	Stomach & other organs	50, 70, 80, 90, 96, 100	1h each	1% wt. I ₂ in 100% EtOH	14h
[19]	Rodent	Brain	20, 50, 70, 90	1h each	1.5% iodine in 90% EtOH	2.5h
[21]	Rodent	Multiple organs	50, 70	1h, 1d or 14d	0.6% Lugol's solution (aqueous I ₂ +KI solution)	18d
[22]	Rodent	Heart	50, 70, 90	1d each	1.5% I ₂ KI in 90% EtOH	72h
[44]	Rodent	Kidney	30, 70	1h each	0.7% PTA + 4% PFA in 70% EtOH	4-18d
[45]	Rodent	Heart & lungs	50, 70, 80, 90, 96, 100	1h each	0.5% I ₂ KI in 100% EtOH	0.5, 1, 1.5, 2, 2.5h
[43]	Rodent	Embryos	30, 50, 70	2d each in 4°C	0.7% PTA in MeOH	6d
[42]	Rodent	Embryos	30, 50, 70	2d each in 4°C	0.5-1.0% PTA in MeOH	4-15d
[14]	Human	Pyloric	30, 50, 70	Not reported	1% PTA in 70% EtOH	8-12w
[49]	Human	Soft tissue	30, 50, 70	1d each	1% PTA in 70% EtOH	5-7d or 2w

Table 2

Details of graded ethanol dehydration and staining protocols from previous literature

A. Graded ethanol dehydration in prior studies

B. Chemical Solution Recipes

B.1. 2% NBF (500 ml)

Ingredient:

- One 1x PBS tablet
- 10% NBF 100 ml
- 400 ml distilled water

Method:

1. Dissolve 1 PBS tablet in 400ml distilled water

Micro-CT Imaging of *Ex-Vivo* Rat Stomachs

2. Add 10% NBF 100 ml

B.2. 0.75% I₂KI (100 ml)

Ingredient:

- 1.5g KI powder
- 0.75g I₂ crystals
- 100ml 70% EtOH

Method:

1. Dissolve KI in 80 ml EtOH.
2. Add Iodine and use a magnetic stirrer to dissolve crystals completely.
3. Add the rest of the 70% EtOH.

B.3. 2% (w/v) PTA (100 ml)

Ingredient:

- 2g PTA
- 100 mL 100% EtOH

Method: Add ingredients together and mix well